Results in Physics 63 (2024) 107867

Contents lists available at ScienceDirect

Results in Physics

journal homepage: www.elsevier.com/locate/rinp

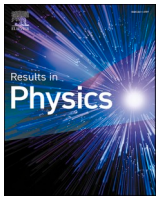

Combination of Fourier transform Jones matrix and beam coherence polarization matrix: Application to a double polarizer rectangular aperture

Ignacio Moreno [a,b,*], David Marco [a,c], María del Mar Sánchez-López [a,d], Juan Campos [e], Angel Lizana [e]

[a] Instituto de Bioingeniería, Universidad Miguel Hernández de Elche, 03202 Elche, Spain
[b] Departamento de Ciencia de Materiales, Óptica y Tecnología Electrónica, Universidad Miguel Hernández de Elche, 03202 Elche, Spain
[c] Aix Marseille Université, CNRS, Centrale Marseille, Institut Fresnel, UMR 7249, 13397 Marseille Cedex 20, France
[d] Departamento de Física Aplicada, Universidad Miguel Hernández de Elche, 03202 Elche, Spain
[e] Departament de Física, Universitat Autònoma de Barcelona, 08193 Bellaterra, Spain

ARTICLE INFO

Keywords:
Polarization
Diffraction
Fourier Transform
Coherence

ABSTRACT

In this work, we extend the Fourier transform Jones (FTJ) matrix approach to handle input scalar fields with spatially variant transverse profiles. Additionally, we integrate the FTJ matrix with the beam coherence-polarization (BCP) matrix, suitable for describing partially coherent and partially polarized light. This approach is particularly effective when the polarization diffractive optical element is illuminated with a quasi-monochromatic paraxial scalar field with transverse spatial coherence, but with any degree of polarization and transverse profile. We apply the method to a meaningful example: a rectangular aperture with orthogonal polarizers on each half, illuminated with uniform randomly polarized light. We provide experimental validation using a randomly polarized He-Ne laser and a specially fabricated double polarizer mask. Furthermore, by placing a polarizer behind the polarization diffractive optical element, we generate a scalar beam with spatial incoherence across two distinct zones, suggesting the potential use of randomly polarized lasers with binary patterned polarizers to encode arbitrary binary coherence functions.

Introduction

The analysis of polarization is a fundamental topic in Optics. While traditionally polarized beams feature a uniform polarization in the beam's cross section, in the last decades there has been a great interest in analyzing vector beams, light beams with a spatial polarization distribution in the transverse plane [1]. Current available technologies based on metamaterials or on liquid-crystals allow to produce diffractive optical elements based on the local modification of the state of polarization [2]. Polarization diffraction gratings [3], polarization-splitting flat lenses [4,5] or q-plates [6] are a few salient examples of such polarization diffractive elements. Indeed, the emergence of these new microfabrication technologies is leading to a revolution in optical design, where a vast number of works dealing with new digital polarization diffractive optical elements (PDOE) and vectorial holographic components [7–9] have recently been reported within the field of structured light [10].

Within the paraxial approximation, the beam coherence-polarization (BCP) matrix [11] is a simplification of the general Wolf's coherence matrix [12], useful to describe propagation of vectorial paraxial quasi-monochromatic fields. This method evaluates the spatial correlations between orthogonal polarization components and is valid for light beams with arbitrary degree of polarization and degree of spatial coherence. The technique has been applied for instance to analyze polarization diffraction gratings under illumination with partially coherent light beams [13,14]. Based on this theory, classical optical Fourier processing systems have been used to control partially coherent light or the degree of polarization [15,16], and the diffraction generated by partially coherent light in the Fourier domain has been analyzed [17].

A complementary simplified approach based on Fourier optics concepts and Jones matrix formalism was proposed for the first time in [18] and probed experimentally in [19], valid for fully polarized quasi-monochromatic plane waves illuminating the PDOE in the paraxial approximation. Initially developed to analyze diffraction from spatial

* Corresponding author at: Instituto de Bioingeniería, Universidad Miguel Hernández de Elche, 03202 Elche, Spain.
E-mail address: i.moreno@umh.es (I. Moreno).

https://doi.org/10.1016/j.rinp.2024.107867
Received 16 April 2024; Received in revised form 4 July 2024; Accepted 5 July 2024
Available online 6 July 2024

light modulators, this Jones matrix generalization of the Fourier optics formalism has recently received a renewed interest as a mathematical advantageous and intuitive tool for designing metamaterials' PDOE without specifying the input polarization state [20,21]. The method calculates the Fourier transform (FT) of each element in the Jones matrix describing the PDOE and provides a description of the diffracted field in terms of a Fourier transformed Jones matrix −which we refer to as Fourier transform Jones (FTJ) matrix- which accounts simultaneously for the polarization transformation in the PDOE plane and in the propagation to the Fourier plane. An enlightening description of how the FTJ formalism relates the scalar, the vector and the matrix regimes can be found in [2].

In this work, we show that the FTJ matrix can be extended to describe beams with arbitrary spatially variant transverse profiles. In addition, we extend the applicability of the FTJ matrix approach by combining it with the BCP matrix, thus modelling a more general scenario where partial spatial coherence or arbitrary degree of polarization can also be considered. The combination is particularly useful when the input beam has any transverse profile and is not fully polarized, but has an arbitrary and spatially uniform state and degree of polarization as well as transverse spatial coherence. We apply the combined FTJ and BCP approach to describe the diffracted field generated by a simple PDOE consisting of a rectangular aperture with two orthogonal linear polarizers superposed on each half aperture. Such diffractive element was introduced by Gori et al in [22] to introduce a scalar treatment for partially polarized beams. We derive analytical relations of the intensity distribution and the state of polarization in the diffracted field when the input light is spatially uniform but fully polarized. Then, we compare the results when the input beam is unpolarized. Finally, in addition to this theoretical analysis, the experimental verification using a patterned polarizer and a randomly polarized laser is presented.

Upon illuminating the patterned polarizer with unpolarized light, the polarization states in each half of the aperture are orthogonal. Each half of the aperture exhibits full coherence with the points within its own region, while demonstrating complete incoherence with respect to points in the opposite half. Introducing another polarizer immediately after the rectangular aperture transforms the vector field into a field with a single well-defined polarization state. Subsequently, after passing through the second polarizer, both halves exhibit the same polarization state. Each half of the aperture then demonstrates full spatial coherence with the points within its respective region, while maintaining complete incoherence with respect to points in the opposite half. The absolute value of the complex degree of correlation of the resulting scalar field was measured. These results indicate the feasibility of generating spatially variant binary spatial coherence patterns, comprising fully correlated areas juxtaposed with uncorrelated zones, through segmented binary polarizers. The segmented polarizer preserves the global amplitude and phase spatially variant functions of the randomly polarized input field, enabling independent selection from the desired binary spatial coherence pattern. Moreover, the technique takes advantage of the fast depolarization dynamics inherent in a randomly polarized laser [23]. Consequently, achieving spatially incoherent binary patterns within shorter temporal periods compared to those provided by rapidly changing digital micro-mirror devices is feasible [24,25], with an energy trade-off.

The paper is organized as follows: after this introduction, Section 2 summarizes the FTJ matrix approach and introduces its extension to describe nonuniform scalar beams. In Section 3 it is applied to analyze the diffraction by the double polarizer aperture under an input quasi-monochromatic fully-polarized plane wave with uniform polarization. Then, Section 4 briefly reviews the BCP formalism and Section 5 presents the combination of the two (FTJ and BCP) approaches. Section 6 provides its application to analyze the diffraction produced by the double polarizer aperture. Section 7 includes the experimental verification using a patterned polarizer and Section 8 extends the experiment to show the coherence properties when a polarizer is included behind the aperture to create a binary uncorrelated scalar pattern. Section 9 presents the conclusions of the work. The work thus represents a useful theoretical and experimental tool to understand the physical insights of diffraction, polarization and coherence, connecting these concepts to classical Fourier optics theory.

The Fourier transform Jones matrix approach

In this section we review the FTJ matrix approach [18] for describing PDOE and extend its applicability to nonuniform beams. Fig. 1 depicts the considered problem. The PDOE plane, which is considered as a thin element, is described by a spatially dependent Jones matrix $\widehat{m}(\mathbf{r})$:

$$\widehat{m}(\mathbf{r}) = \begin{pmatrix} m_{xx}(\mathbf{r}) & m_{xy}(\mathbf{r}) \\ m_{yx}(\mathbf{r}) & m_{yy}(\mathbf{r}) \end{pmatrix}, \tag{1}$$

where $m_{\alpha\beta}(\mathbf{r})$, $\alpha,\beta = x,y$, are the Jones matrix elements which, in general, are complex-valued functions, and $\mathbf{r} = (x,y)$ denotes the spatial coordinates in the PDOE transversal plane. This diffractive element is illuminated with a fully coherent and fully polarized input paraxial field, but with a spatially-variant state of polarization. The transverse spatial properties of the field are described by the Jones vector $\mathbf{e}_1(\mathbf{r}) = \left[\mathrm{e}_{1x}(\mathbf{r})\mathrm{e}_{1y}(\mathbf{r})\right]^T$, where e_{1x} and e_{1y} are the transverse spatial electric field components in the x and y directions. Then, the beam right behind the PDOE is given by $\mathbf{e}_2(\mathbf{r}) = \widehat{m}(\mathbf{r})\mathbf{e}_1(\mathbf{r})$.

To obtain the field in the Fourier domain, we consider the usual approximations in Fourier optics [26]: the paraxial approximation and the assumption that the spatial variations in the PDOE are larger than the wavelength. In this situation, the diffracted field in the Fourier plane (obtained either by free propagation in the Fraunhofer approximation or by a lens system) can be described by a Jones vector $\mathbf{E}_2(\mathbf{u})$ whose components are given by $\mathrm{E}_{2\alpha}(\mathbf{u}) = \mathscr{F}^{(2)}[\mathbf{e}_{2\alpha}(\mathbf{r})]$, where the subindex $\alpha = x,y$ indicates the electric field components in the horizontal and vertical directions and $\mathscr{F}^{(2)} \equiv \mathscr{F}_{\mathbf{r}\to\mathbf{u}}$ indicates the 2D Fourier transform typically used in diffraction problems, that maps the spatial coordinates $\mathbf{r} = (x,y)$ to the spatial frequencies $\mathbf{u} = (u,v)$. We write this relation compactly as $\mathbf{E}_2(\mathbf{u}) = \mathscr{F}^{(2)}[\mathbf{e}_2(\mathbf{r})]$ understanding that the Fourier transform applied to each component of the Jones vector. Thus, $\mathbf{E}_2(\mathbf{u})$ can be calculated as

$$\mathbf{E}_2(\mathbf{u}) = \mathscr{F}^{(2)}[\mathbf{e}_2(\mathbf{r})] = \mathscr{F}^{(2)}\left[\begin{pmatrix} m_{xx}(\mathbf{r})\mathrm{e}_{1x}(\mathbf{r}) + m_{xy}(\mathbf{r})\mathrm{e}_{1y}(\mathbf{r}) \\ m_{yx}(\mathbf{r})\mathrm{e}_{1x}(\mathbf{r}) + m_{yy}(\mathbf{r})\mathrm{e}_{1y}(\mathbf{r}) \end{pmatrix}\right]. \tag{2}$$

Considering the FT properties, this relation can be written as:

$$\mathbf{E}_2(\mathbf{u}) = \begin{pmatrix} M_{xx}(\mathbf{u})*\mathrm{E}_{1x}(\mathbf{u}) + M_{xy}(\mathbf{r})*\mathrm{E}_{1y}(\mathbf{u}) \\ M_{yx}(\mathbf{u})*\mathrm{E}_{1x}(\mathbf{u}) + M_{yy}(\mathbf{u})*\mathrm{E}_{1y}(\mathbf{u}) \end{pmatrix}, \tag{3}$$

where * indicates the convolution operation, $M_{\alpha\beta}(\mathbf{u}) = \mathscr{F}^{(2)}[m_{\alpha\beta}(\mathbf{r})]$ and $\mathrm{E}_{1\alpha}(\mathbf{u}) = \mathscr{F}^{(2)}[\mathrm{e}_{1\alpha}(\mathbf{r})]$, $\alpha,\beta = x,y$. Functions $\mathrm{E}_{1\alpha}(\mathbf{u})$ are the two components of the Fourier transformed input Jones vector, $\mathbf{E}_1(\mathbf{u}) = \mathscr{F}^{(2)}[\mathbf{e}_1(\mathbf{r})]$ and functions $M_{\alpha\beta}(\mathbf{u})$ define the FTJ matrix $\widehat{M}(\mathbf{u})$ that characterizes the PDOE in the Fourier domain as:

$$\widehat{M}(\mathbf{u}) = \mathscr{F}^{(2)}[\widehat{m}(\mathbf{r})] = \begin{pmatrix} M_{xx}(\mathbf{u}) & M_{xy}(\mathbf{u}) \\ M_{yx}(\mathbf{u}) & M_{yy}(\mathbf{u}) \end{pmatrix}. \tag{4}$$

Then, Eq. (3) can be rewritten in a compact way as:

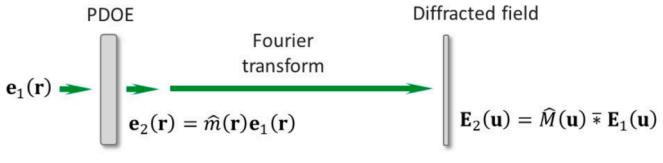

Fig. 1. Scheme of the polarization transformations in the Jones-Fourier matrix method.

$$\mathbf{E}_2(\mathbf{u}) = \widehat{M}(\mathbf{u}) \overline{*} \mathbf{E}_1(\mathbf{u}), \tag{5}$$

where the symbol $\overline{*}$ denotes the usual matrix product, but where regular scalar multiplications between two functions are substituted by convolutions, so the result in Eq. (3) is retrieved. Note that the matrix $\widehat{M}(\mathbf{u})$ contains the full information of the PDOE element, described in the Fourier domain, thus containing the propagation. This matrix is independent of the input beam characteristics, which are described by $\mathbf{E}_1(\mathbf{u})$.

Equation (5) can be further simplified if the input beam has uniform polarization. Then the input Jones vector can be written as $\mathbf{e}_1(\mathbf{r}) = \mathbf{e}_1 a(\mathbf{r})$, where $\mathbf{e}_1$ is a constant Jones vector, independent of $\mathbf{r}$, and $a(\mathbf{r})$ is a complex scalar function providing the beam amplitude and phase spatial profile. In this case, $\mathbf{E}_2(\mathbf{u})$ is

$$\mathbf{E}_2(\mathbf{u}) = \widehat{M}_{\mathrm{A}}(\mathbf{u})\mathbf{e}_1, \tag{6}$$

where $\widehat{M}_{\mathrm{A}}(\mathbf{u}) = \mathscr{F}^{(2)}[\widehat{m}(\mathbf{r})a(\mathbf{r})] = \widehat{M}(\mathbf{u})*A(\mathbf{u})$ with $A(\mathbf{u}) = \mathscr{F}^{(2)}[a(\mathbf{r})]$. Equation (6) provides the diffracted field as the standard Jones matrix multiplication of $\widehat{M}_{\mathrm{A}}(\mathbf{u})$ by $\mathbf{e}_1$, which describes the polarization state of the input field. Matrix $\widehat{M}_{\mathrm{A}}(\mathbf{u})$ characterizes the PDOE and the input field profile as long as the latter remains unchanged, regardless of the input polarization state. When the beam is considered a plane wave ($a(\mathbf{r}) = 1$), the propagated field can be computed simply as the product of the FTJ matrix in Eq. (4) (containing exclusively information about the PDOE) by the input constant Jones vector $\mathbf{e}_1$, which solely describes the input field:

$$\mathbf{E}_2(\mathbf{u}) = \widehat{M}(\mathbf{u})\mathbf{e}_1. \tag{7}$$

Such a simplification, despite being strong, explains rich polarization and diffraction phenomena, as shown next with a simple example.

Application to a double polarizer rectangular aperture

Fig. 2(a) shows the rectangular aperture proposed by Gori *et al* in [22], which is taken to illustrate the method for an input plane wave. It is a square aperture of size a, where the left half is covered with a vertical linear polarizer, while the right half is covered with a horizontal polarizer. For simplicity we consider only the variation along the horizontal dimension. The Jones matrix describing this PDOE is given by:

$$\begin{aligned}\widehat{m}(\mathbf{r}) &= \mathrm{rect}\left(\frac{x-a/4}{a/2}\right)\begin{pmatrix}1 & 0\\ 0 & 0\end{pmatrix} + \mathrm{rect}\left(\frac{x+a/4}{a/2}\right)\begin{pmatrix}0 & 0\\ 0 & 1\end{pmatrix}\\ &= \begin{pmatrix}\mathrm{rect}\left(\dfrac{x-a/4}{a/2}\right) & 0\\ 0 & \mathrm{rect}\left(\dfrac{x+a/4}{a/2}\right)\end{pmatrix},\end{aligned} \tag{8}$$

where the rectangle function is defined as $\mathrm{rect}(x) = 1$ if $|x| \le 1/2$ and $\mathrm{rect}(x) = 0$ elsewhere. The corresponding Fourier-Jones matrix is given by:

$$\widehat{M}(u) = \frac{a}{2}\mathrm{sinc}\left(\frac{au}{2}\right)\begin{pmatrix}e^{-i\pi au/2} & 0\\ 0 & e^{+i\pi au/2}\end{pmatrix}, \tag{9}$$

where $\mathrm{sinc}(u) = \mathscr{F}[\mathrm{rect}(x)] = \sin(\pi u)/(\pi u)$.

The Jones matrix in Eq. (9) provides the physical insight of the polarization transformation that occurs in the aperture and upon propagation to the Fourier plane. Note that the same matrix is valid for any input state of polarization, thus giving a complete description of the PDOE and the pattern that generates. The sinc term in Eq. (9) acts as an envelope function that is the Fourier transform of a rectangular aperture of width $a/2$, i.e., one of the two polarizer apertures. Its first null occurs at the spatial frequency $u = \pm 2/a$. The Jones matrix on the right part of Eq. (9) describes a linear retarder with neutral axes aligned along the $x-y$ axes, and with a retardance that depends on the spatial frequency u and the aperture size a as $\phi(u) = \pi a u$.

Therefore, if the aperture in Fig. 2(a) is illuminated with a fully polarized quasi-monochromatic plane wave with a linear polarization oriented at 45°, the two aperture halves feature the same intensity transmission, but the light right after the aperture is polarized vertically in the left half, and horizontally in the right part.

Using Eq. (7), the diffracted field in the FT plane is given by the following Jones vector:

$$\mathbf{E}_2(u) = \widehat{M}(u)\frac{1}{\sqrt{2}}\begin{pmatrix}1\\ 1\end{pmatrix} = \frac{a}{2}\mathrm{sinc}\left(\frac{au}{2}\right)\frac{1}{\sqrt{2}}\begin{pmatrix}e^{-i\pi au/2}\\ e^{+i\pi au/2}\end{pmatrix}. \tag{10}$$

The diffracted field intensity (understood as the modulus square of the electric field) is:

$$I(u) = \mathbf{E}_2^{\dagger}(u)\cdot\mathbf{E}_2(u) = \frac{a^2}{4}\mathrm{sinc}^2\left(\frac{au}{2}\right), \tag{11}$$

where the dagger † indicates the Hermitian conjugate. The diffracted field intensity $I(u)$ in Eq. (11) is shown as the black curve in Fig. 2(b).

Equation (10) also provides the state of polarization, given by the normalized Jones vector $(1/\sqrt{2})\begin{pmatrix}e^{-i\pi au/2} & e^{+i\pi au/2}\end{pmatrix}^T$ where T denotes the transposed matrix. The center of the diffracted field ($u = 0$) is linearly polarized oriented at 45°, like the input polarization. At spatial frequencies $u = \pm 1/a$ the retardance becomes $\phi(u) = \pm\pi$, i.e., equivalent to a half-wave retarder. Therefore, the state of polarization at these points is linear but oriented at −45°. On the contrary, at spatial frequencies $u = \pm 1/2a$ and $u = \pm 3/2a$ the retardance is $\phi(u) = \pm\pi/2$ and $\phi(u) = \pm 3\pi/2$ respectively, i.e., equivalent to a quarter-wave and a three-quarter wave retarder. Therefore, the polarizations are circular at these locations. In the rest of the diffracted field, the polarization

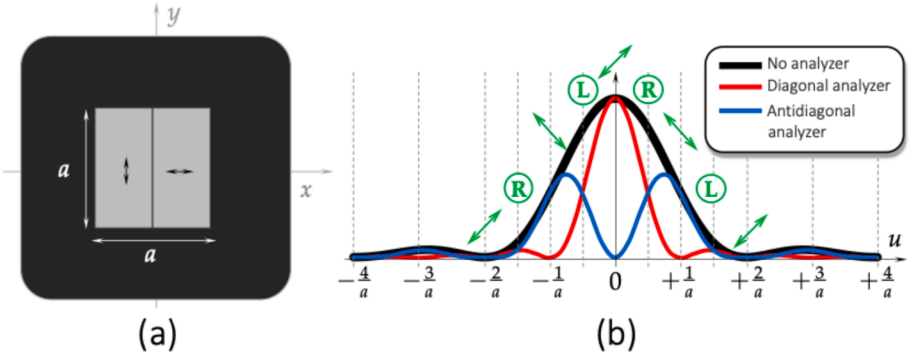

Fig. 2. (a) PDOE consisting in a square aperture with two orthogonal linear polarizers in each half side. (b) Horizontal profile of the diffracted field when illuminating the PDOE with a plane wave with uniform linear polarization oriented at 45°.

progressively changes ellipticity with u, but the azimuth remains aligned along $\pm 45°$. At the spatial frequencies $u = \pm 2/a$, where the first intensity nulls occur, the state of polarization would be again linear oriented at $+45°$. These polarization states are indicated on top of the sinc squared function in Fig. 2(b).

The additional red and blue curves shown in Fig. 2(b) correspond to the intensity of the diffracted field resulting from projecting the Jones vector in Eq. (10) onto a linear polarizer analyzer oriented either diagonal ($+45°$) or antidiagonal ($-45°$) respectively. For the case of the diagonal analyzer, the two halves of the aperture project in the same way onto the analyzer transmission axis. Therefore, the result (red curve in Fig. 2(b)) is equivalent to the scalar diffraction from the complete rectangular aperture of width a, i.e., a sinc squared curve whose central lobe reaches zero intensity at spatial frequencies $u = \pm 1/a$ (note that at these spatial frequencies is where the diffracted field becomes linearly polarized at $-45°$, i.e., crossed with respect to the analyzer). On the contrary, when the analyzer is oriented antidiagonal ($-45°$), the intensity shows a zero at the center, where the state of polarization is diagonal, and exhibits two lateral lobes before reaching the next null points at frequencies $u = \pm 2/a$. The explanation is that the vertical and horizontal polarizations project in opposite direction onto the antidiagonal analyzer transmission axis, thus resulting in a π phase shift between the contribution of each half aperture in Fig. 2(a), thus changing the interference condition.

It is interesting noting that the above analysis of the double polarizer rectangular aperture can be applied directly extended to problems with circular symmetry. Let us consider an aperture with circular symmetry and maximum radius R whose transmission is described with a scalar complex function $m(r)$, r being the radial coordinate, illuminated with a plane wave. Then, by defining the variable $s = (r/R)^2 - 0.5$, the transmission function is described by a function $m(s)$ that varies from -0.5 to $+0.5$ and the diffracted field distribution along the propagation axis can be calculated with the following 1D Fourier transform [27,28]:

$$E(\rho = 0, W_{20}) = \frac{1}{2}\exp(i\pi W_{20}) \int_{-0.5}^{+0.5} m(s)\exp(i2\pi s W_{20})ds, \tag{12}$$

where ρ is the normalized radial coordinate in the Fourier transform plane, and W_{20} is the defocus parameter typically employed to calculate the point spread function (PSF) in defocused planes. This W_{20} parameter is related to the propagation distance z around the focusing plane as $W_{20} = (NA^2/2\lambda)z$, where NA is the numerical aperture of the lens focusing the beam and λ is the wavelength [29]. Since the function $m(s)$ is null outside the limits of integration in Eq. (12), these limits can be extended to infinity and the Fourier transform relation $E(W_{20}) \propto \mathscr{F}^{(1)}[m(s)]$ can be concluded, where $\mathscr{F}^{(1)} \equiv \mathscr{F}_{s \to W_{20}}$ now indicates the 1D FT mapping the variable s and the defocus parameter W_{20}.

This is a well-known result from the theory of imaging apodizing filters that was extended to a binary polarization apodizer in [29]. Fig. 3 illustrates the case for a circular aperture of maximum radius R consisting in a central disc of radius $R/\sqrt{2}$ with a vertical polarizer and an annulus of horizontal polarizer for $r \in (R/\sqrt{2}, R]$. This aperture can be described by a Jones matrix $\widehat{m}(r)$, which after the coordinate transformation $s = (r/R)^2 - 0.5$ is described with a matrix $\widehat{m}(s)$ that is formally equivalent to that in Eq. (8). Therefore, all the conclusions derived in this section, in particular the intensity and polarization distribution in Fig. 2(b), can be directly extended by analogy to the axial distribution ($\rho = 0$) when substituting the spatial frequency u by the defocus parameter W_{20}.

The beam coherence-polarization (BCP) matrix approach

If the aperture in Fig. 2(a) is illuminated with a quasi-monochromatic unpolarized plane wave, the polarization distribution right after the aperture is the same as in the previous case with illumination with linearly polarized light oriented at 45°. In both cases, the two rectangles transmit half of the input intensity and light is linearly polarized vertical / horizontal on the left / right rectangle. However, the spatial coherence properties are very different. The previous FTJ matrix approach cannot be applied directly with either non-fully coherent non-fully polarized light. In this situation the BCP matrix [11] is suitable.

Given a quasi-monochromatic paraxial electric field whose transverse spatial and temporal variation at a given plane is defined by the vector $\mathbf{e}_1(\mathbf{r}, t) = \left(\mathrm{e}_x(\mathbf{r}, t)\mathrm{e}_y(\mathbf{r}, t)\right)^T$, the BCP matrix at this plane is defined as

$$\widehat{j}(\mathbf{r}_a, \mathbf{r}_b) = \langle \mathbf{e}_1(\mathbf{r}_a, t)\mathbf{e}_1^{\dagger}(\mathbf{r}_b, t)\rangle = \begin{pmatrix} j_{xx}(\mathbf{r}_a, \mathbf{r}_b) & j_{xy}(\mathbf{r}_a, \mathbf{r}_b) \\ j_{yx}(\mathbf{r}_a, \mathbf{r}_b) & j_{yy}(\mathbf{r}_a, \mathbf{r}_b) \end{pmatrix}, \tag{13}$$

where $j_{\alpha\beta}(\mathbf{r}_a, \mathbf{r}_b) = \left\langle \mathrm{e}_\alpha(\mathbf{r}_a, t)\mathrm{e}_\beta^*(\mathbf{r}_b, t)\right\rangle$ are the correlations between the α, $\beta = x, y$ electric field components at transversal locations $\mathbf{r}_a$ and $\mathbf{r}_b$, and $\langle \bullet \rangle$ denotes time averaging. If the BCP matrix is evaluated at the same location, the result is the spatially variant polarization matrix $\widehat{p}(\mathbf{r}) = \widehat{j}(\mathbf{r} = \mathbf{r}_a = \mathbf{r}_b)$, which provides information about the local polarization properties of the field. The total intensity of the field described by Eq. (12) is obtained as:

$$I(\mathbf{r}) = \mathrm{Tr}[\widehat{p}(\mathbf{r})] = j_{xx}(\mathbf{r}) + j_{yy}(\mathbf{r}), \tag{14}$$

where $\mathrm{Tr}[\bullet]$ stands for the trace of the matrix. The degree of polarization is given by

$$p(\mathbf{r}) = \sqrt{1 - \frac{4\mathrm{Det}[\widehat{p}(\mathbf{r})]}{\{\mathrm{Tr}[\widehat{p}(\mathbf{r})]\}^2}}, \tag{15}$$

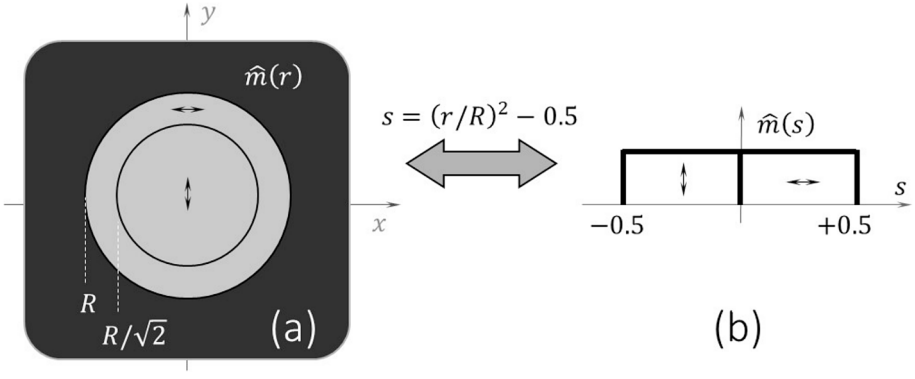

Fig. 3. (a) PDOE consisting in a circular aperture with a central disc with vertical polarizer surrounded by an annulus of horizontal polarizer. (b) Corresponding one dimensional function after coordinate transformation $s = (r/R)^2 - 0.5$.

where Det[•] stands for the determinant of the matrix.

Let us highlight that the BCP matrix characterizes the light beam, while the Jones matrix characterizes an optical element transforming the polarization. The transformation rule for the BCP matrix of a light beam when traversing a polarization element characterized by a Jones matrix $\widehat{m}(\mathbf{r})$ is [11]:

$$\widehat{j}_2(\mathbf{r}_a,\mathbf{r}_b)=\widehat{m}(\mathbf{r}_a)\widehat{j}_1(\mathbf{r}_a,\mathbf{r}_b)\widehat{m}^{\dagger}(\mathbf{r}_b). \tag{16}$$

Then, the diffracted field in the FT plane has electric field components given by $\mathrm{E}_{2\alpha}(\mathbf{u},t)=\mathscr{F}[\mathrm{e}_{2\alpha}(\mathbf{r},t)]$, leading to a $\widehat{J}_2(\mathbf{u}_a,\mathbf{u}_b)$ matrix whose elements are given by the FT and inverse FT of the corresponding elements of $\widehat{j}_2(\mathbf{r}_a,\mathbf{r}_b)$ over the $\mathbf{r}_a$ and $\mathbf{r}_b$ coordinates [11,12]:

$$\begin{aligned}J_{2\alpha\beta}(\mathbf{u}_a,\mathbf{u}_b)&=\left\langle \mathrm{E}_{2\alpha}(\mathbf{u}_a,t)\mathrm{E}^{*}_{2\beta}(\mathbf{u}_b,t)\right\rangle=\iint_{-\infty}^{+\infty}j_{2\alpha\beta}(\mathbf{r}_a,\mathbf{r}_b)e^{-i2\pi(\mathbf{r}_a\cdot\mathbf{u}_a-\mathbf{r}_b\cdot\mathbf{u}_b)}\mathrm{d}\mathbf{r}_a\mathrm{d}\mathbf{r}_b\\&=\mathscr{F}^{(4)}\left[j_{2\alpha\beta}(\mathbf{r}_a,\mathbf{r}_b)\right],\end{aligned} \tag{17}$$

where $\mathscr{F}^{(4)}\equiv\mathscr{F}_{(\mathbf{r}_a,\mathbf{r}_b)\to(\mathbf{u}_a,-\mathbf{u}_b)}$ indicated in the last part of the equation means that the operation is a 4D Fourier transform where the coordinates $\mathbf{r}_a$ and $\mathbf{r}_b$ are mapped to the spatial frequencies $\mathbf{u}_a$ and $-\mathbf{u}_b$, respectively. This process is illustrated in Fig. 4. Note that for consistency we denote with capital letters J the BCP matrix and its elements in the Fourier domain while we use j to denote the BCP matrix and its elements in the spatial domain.

Combination of the FTJ and BCP matrix approaches

We next derive a theoretical framework that combines both FTJ and BCP matrix approaches. The components of the matrix in Eq. (16) are given by $j_{2\alpha\beta}(\mathbf{r}_a,\mathbf{r}_b)=m_{\alpha\gamma}(\mathbf{r}_a)j_{1\gamma\delta}(\mathbf{r}_a,\mathbf{r}_b)m^{\dagger}_{\delta\beta}(\mathbf{r}_b)$, where we use Einstein's summation convention, implying summation over repeated indices without explicitly writing the summation symbol. We substitute these terms into Eq. (17) and assume that the PDOE does not depend on time, so the elements of the matrix $\widehat{m}$ describing the PDOE are constant during the temporal average for each value $J_{2\alpha\beta}(\mathbf{u}_a,\mathbf{u}_b)$. This allows us to express the matrix components in Eq. (17) as:

$$J_{2\alpha\beta}(\mathbf{u}_a,\mathbf{u}_b)=\mathscr{F}^{(4)}\left[m_{\alpha\gamma}(\mathbf{r}_a)\right]*\mathscr{F}^{(4)}\left[j_{1\gamma\mu}(\mathbf{r}_a,\mathbf{r}_b)\right]*\mathscr{F}^{(4)}\left[m^{\dagger}_{\mu\beta}(\mathbf{r}_b)\right], \tag{18}$$

where again these 4D Fourier transforms must consider the mapping $\mathscr{F}_{(\mathbf{r}_a,\mathbf{r}_b)\to(\mathbf{u}_a,-\mathbf{u}_b)}$, as in Eq. (17). The entries $\mathscr{F}^{(4)}\left[j_{1\gamma\delta}(\mathbf{r}_a,\mathbf{r}_b)\right]$ are the components of the BCP matrix of the propagated input beam, i.e.:

$$\widehat{J}_1(\mathbf{u}_a,\mathbf{u}_b)=\iint_{-\infty}^{+\infty}\widehat{j}_1(\mathbf{r}_a,\mathbf{r}_b)e^{-i2\pi(\mathbf{r}_a\cdot\mathbf{u}_a-\mathbf{r}_b\cdot\mathbf{u}_b)}\mathrm{d}\mathbf{r}_a\mathrm{d}\mathbf{r}_b=\mathscr{F}^{(4)}[\widehat{j}_1(\mathbf{r}_a,\mathbf{r}_b)], \tag{19}$$

This matrix contains information on the polarization and spatial coherence of the input beam illuminating the PDOE, described in the FT domain.

The 4D FTs regarding the matrix components of the PDOE can be expressed as 2D FTs: $\mathscr{F}^{(4)}\left[m_{\alpha\gamma}(\mathbf{r}_a)\right]=\mathscr{F}^{(2)}_{\mathbf{r}_a\to\mathbf{u}_a}\left[m_{\alpha\gamma}(\mathbf{r}_a)\right]\delta(\mathbf{u}_b)$ and $\mathscr{F}^{(4)}\left[m^{\dagger}_{\mu\beta}(\mathbf{r}_b)\right]=\mathscr{F}^{(2)}_{\mathbf{r}_b\to-\mathbf{u}_b}\left[m^{\dagger}_{\mu\beta}(\mathbf{r}_b)\right]\delta(\mathbf{u}_a)$, where δ represents the Dirac delta distribution. These are elements of the matrices

$$\widehat{M}(\mathbf{u}_a)=\int_{-\infty}^{\infty}\widehat{m}(\mathbf{r}_a)e^{-i2\pi\mathbf{r}_a\cdot\mathbf{u}_a}\mathrm{d}\mathbf{r}_a=\mathscr{F}^{(2)}_{\mathbf{r}_a\to\mathbf{u}_a}[\widehat{m}(\mathbf{r}_a)], \tag{20a}$$

$$\widehat{M}^{\dagger}(\mathbf{u}_b)=\int_{-\infty}^{\infty}\widehat{m}^{\dagger}(\mathbf{r}_b)e^{+i2\pi\mathbf{r}_b\cdot\mathbf{u}_b}\mathrm{d}\mathbf{r}_b=\mathscr{F}^{(2)}_{\mathbf{r}_b\to-\mathbf{u}_b}[\widehat{m}^{\dagger}(\mathbf{r}_b)], \tag{20b}$$

which are analogous to the FTJ matrix discussed in Section 2. The matrix of the propagated field after the PDOE can then be written as:

$$\widehat{J}_2(\mathbf{u}_a,\mathbf{u}_b)=[\widehat{M}(\mathbf{u}_a)\delta(\mathbf{u}_b)]\overline{*}\,\widehat{J}_1(\mathbf{u}_a,\mathbf{u}_b)\overline{*}[\widehat{M}^{\dagger}(\mathbf{u}_b)\delta(\mathbf{u}_a)]. \tag{21}$$

where the symbol $\overline{*}$ denotes again the matrix multiplication where standard products are substituted by convolutions.

The above relation in Eq. (21) can be further simplified in a limiting case that matches our experiment in Section 7. We consider an input beam that is transversely spatially coherent with uniform polarization state and uniform degree of polarization. Therefore, the transverse spatial and temporal properties of the input field are separable and can be described with a vector $\mathbf{e}_1(\mathbf{r},t)=a(\mathbf{r})\mathbf{e}_1(t)$, where $a(\mathbf{r})$ is a complex scalar function of the transverse position, and $\mathbf{e}_1(t)$ is a vector that only depends on time. The corresponding input BCP matrix is then also separable as $\widehat{j}_1(\mathbf{r}_a,\mathbf{r}_b)=a(\mathbf{r}_a)a^{*}(\mathbf{r}_b)\widehat{p}_1$ where $\widehat{p}_1=\langle\mathbf{e}_1(t)\mathbf{e}_1^{\dagger}(t)\rangle$ is the constant polarization matrix describing the uniform polarization of the input beam, which now can have arbitrary degree of polarization. Then Eq. (19) can be written as

$$\widehat{J}_2(\mathbf{u}_a,\mathbf{u}_b)=\widehat{M}_{\mathrm{A}}(\mathbf{u}_a)\widehat{p}_1\widehat{M}^{\dagger}_{\mathrm{A}}(\mathbf{u}_b), \tag{22}$$

where $\widehat{M}_{\mathrm{A}}(\mathbf{u})=\mathscr{F}^{(2)}[\widehat{m}(\mathbf{r})a(\mathbf{r})]=\widehat{M}(\mathbf{u})*A(\mathbf{u})$, as described after Eq. (6). As mentioned in Section 2, this matrix contains the information about the input beam and the PDOE and it is separable from the input beam polarization. This approach thus extends the applicability of the FTJ matrix to input scalar quasi-monochromatic light with transverse spatial coherence, but that can be partially polarized and have any transverse profile.

In the case of an input plane wave, taking $a(\mathbf{r})=1$, the above equation can be further simplified to:

$$\widehat{J}_2(\mathbf{u}_a,\mathbf{u}_b)=\widehat{M}(\mathbf{u}_a)\widehat{p}_1\widehat{M}^{\dagger}(\mathbf{u}_b). \tag{23}$$

This relation thus gives the BCP matrix in the Fourier plane, now calculated as the usual transformation rule of the BCP matrix expressed in Eq. (16) but now using the FTJ matrix $\widehat{M}(\mathbf{u})$ in Eq. (4) that characterizes the PDOE in the Fourier domain. This way the diffracted field can be calculated directly, simultaneously accounting for the action of the PDOE on the input beam and for the propagation, as indicated in Fig. 3.

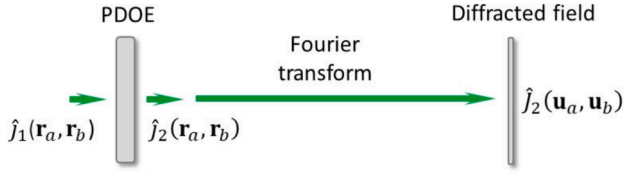

Fig. 4. Scheme equivalent to that in Fig. 1considering the BCP matrix.

Application to analyze the double polarizer rectangular aperture

To illustrate the combined FJT and BCP method, let us consider again the PDOE in Fig. 2(a), which is described by the FTJ matrix in Eq. (4). We regard two cases that can be easily implemented experimentally, as described in the next section. In both cases, the input light beam is considered a plane wave, so Eq. (23) can be applied. We compare the situation when it is fully polarized with linear polarization at 45°, with a second case where the beam is fully unpolarized. In both cases, the spatial distribution of the intensity and polarization states right after the aperture is the same, but the diffracted field is very different, as shown next.

Case 1: Illumination with linearly polarized light oriented at 45°

This case was already analyzed in Section 2 within the Jones matrix Fourier optics formalism, and it is included here to show that the same results are obtained. The BCP matrix for this input light beam is

$$\widehat{p}_1 = \frac{1}{2}\begin{pmatrix} 1 & 1 \\ 1 & 1 \end{pmatrix}. \tag{24}$$

The BCP matrix at the Fourier plane is obtained with Eq. (23) using the FTJ matrix in Eq. (9):

$$\widehat{J}_2(u_a,u_b) = \frac{a^2}{8}\mathrm{sinc}\left(\frac{au_a}{2}\right)\mathrm{sinc}\left(\frac{au_b}{2}\right)\begin{pmatrix} e^{-i\pi a(u_a-u_b)/2} & e^{-i\pi a(u_a+u_b)/2} \\ e^{+i\pi a(u_a+u_b)/2} & e^{+i\pi a(u_a-u_b)/2} \end{pmatrix}. \tag{25}$$

If we are only interested in the intensity and polarization distribution, we can directly use the polarization matrix $\widehat{p}_2(\mathbf{u})$ obtained by considering $u = u_a = u_b$, leading to

$$\widehat{p}_2(\mathbf{u}) = \frac{a^2}{8}\mathrm{sinc}^2\left(\frac{au}{2}\right)\begin{pmatrix} 1 & e^{-i\pi au} \\ e^{+i\pi au} & 1 \end{pmatrix}. \tag{26}$$

The intensity $I(u) = \mathrm{Tr}[\widehat{p}_2(u)\,] = \frac{1}{4}a^2\mathrm{sinc}^2(au/2)$ coincides with the result already derived in Eq. (11), and the degree of polarization (Eq. (14)) is $p(u) = 1$ at all points. The local normalized state of polarization is given by the polarization matrix normalized by the intensity, i.e.:

$$\frac{\widehat{p}_2(u)}{I(u)} = \frac{1}{2}\begin{pmatrix} 1 & e^{-i\pi au} \\ e^{+i\pi au} & 1 \end{pmatrix}. \tag{27}$$

This reveals that the polarization depends on the spatial frequency u in the same manner as shown in Fig. 2(b) since the normalized Jones vector in Eq. (10) provides exactly the polarization matrix in Eq. (27) when calculating $\mathbf{E}_2(u)\mathbf{E}_2^{\dagger}(u)$.

Therefore, these calculations recover the results previously obtained with the FTJ matrix approach, as it should be expected for a fully polarized input quasi-monochromatic plane wave.

Case 2: Illumination with unpolarized light

We now consider the situation of an input totally unpolarized quasi-monochromatic plane wave. Note that this case cannot be treated directly with the FTJ approach. Now the input BCP matrix is

$$\widehat{p}_1 = \frac{1}{2}\begin{pmatrix} 1 & 0 \\ 0 & 1 \end{pmatrix}, \tag{28}$$

and the corresponding BCP matrix at the Fourier plane (Eq. (22)) is directly given by $\widehat{J}_2(\mathbf{u}_a,\mathbf{u}_b) = \frac{1}{2}\widehat{M}(\mathbf{u}_a)\widehat{M}^{\dagger}(\mathbf{u}_b)$, which leads to

$$\widehat{J}_2(u_a,u_b) = \frac{a^2}{8}\mathrm{sinc}\left(\frac{au_a}{2}\right)\mathrm{sinc}\left(\frac{au_b}{2}\right)\begin{pmatrix} e^{-i\pi a(u_a-u_b)/2} & 0 \\ 0 & e^{+i\pi a(u_a-u_b)/2} \end{pmatrix}. \tag{29}$$

Note the difference with respect to Eq. (25) in the off-diagonal elements, which are now zero indicating the null correlation between the x and y components of the electric field. Again, we consider $u = u_a = u_b$ to calculate the polarization matrix:

$$\widehat{p}_2(u) = \frac{a^2}{8}\mathrm{sinc}^2\left(\frac{au}{2}\right)\begin{pmatrix} 1 & 0 \\ 0 & 1 \end{pmatrix}, \tag{30}$$

which shows that the diffracted field is now unpolarized at all points ($p(u) = 0$). The intensity $I(u) = \mathrm{Tr}[\widehat{p}_2(u)\,]$ provides the same result as in Eq. (11):

$$I(u) = \mathrm{Tr}[\widehat{p}_2(u)\,] = \frac{a^2}{4}\mathrm{sinc}^2\left(\frac{au}{2}\right). \tag{31}$$

These results under unpolarized illumination reveal some interesting features with respect to the previous case: (i) the intensity of the diffracted field is the same, but (ii) the diffracted field is now completely unpolarized at all points. The physical explanation is related to the correlation between the electric field components e_x and e_y at different points of the aperture. When the aperture is illuminated with unpolarized light, there is no correlation between the electric field component e_y transmitted at points on the left part of the aperture with e_x transmitted at points on the right part of the aperture. As a consequence, the two halves are mutually incoherent, and the diffracted field is the incoherent superposition of the two diffraction patterns corresponding to rectangular apertures of width $a/2$, one with vertical polarization and the other one with horizontal polarization. Although the unpolarized input light becomes fully polarized right after the aperture due to the polarizers, the propagation results in a diffracted field that remains unpolarized at all points. This occurs due to the incoherent superposition of two equal diffracted patterns with orthogonal polarizations.

Experimental verification

In this section we present a simple experiment to probe the above-described theory. Fig. 5 shows a scheme of the optical setup. As light source we use a continuous wave (CW) randomly polarized He-Ne laser (Melles-Griot 05-LGR-193), having a wavelength of 543 nm and 0.5 mW power. Two sets of orthogonal linearly polarized longitudinal modes with slightly different frequencies are generated by the laser, causing the resulting polarization ellipse to rapidly vary on a nanosecond time scale. The laser is spatially filtered and collimated by means of lens (L1), so we consider that the light beam after L1 is quasi-monochromatic, unpolarized, and has transverse spatial coherence. A linear polarizer (Pol) is added before the spatial filter when the input light must be fully polarized. The key element is the optical component developed by Codixx [30] consisting in two rectangular polarizers placed side by side, one aligned vertically and the other horizontally.

Each rectangle has a size of 5 mm × 10 mm, with a gap between them slightly less than 0.1 mm. This double polarizer element could serve as the aperture described in Fig. 2(a). However, its dimensions are rather big, so the diffractive pattern would be very small. Thus, to better visualize the effects and to achieve an accurate control on the aperture dimensions, we inserted a slit of adjustable width (Owis SP60). Since the slit mount prevents us from placing the double polarizer right after the slit, we use a relay optics system, composed by lenses L2 and L3, to image the adjustable slit onto the Codixx polarizer plane. Finally, lens L4 focuses the FT on a camera. Since we are interested in evaluating the polarization spatial distribution of the diffracted field, we employ a detection system consisting in a polarization state analyzer (PSA) composed of a polarization camera and a quarter-wave plate (QWP) [31]. The polarization camera (Thorlabs CS505MUP Kiralux) is a monochrome sensor with 2448 × 2048 square pixels of 3.45 μm side. The sensor includes an integrated micro-polarizer array attached to the pixel detectors that captures in a single shot the images for horizontal (H), vertical (V), diagonal (D) and antidiagonal (A) linear analyzers. A QWP is included before the camera to measure the circular polarization components. The camera also provides the total intensity capture (as if measured without analyzers) by summing the images for crossed analyzers.

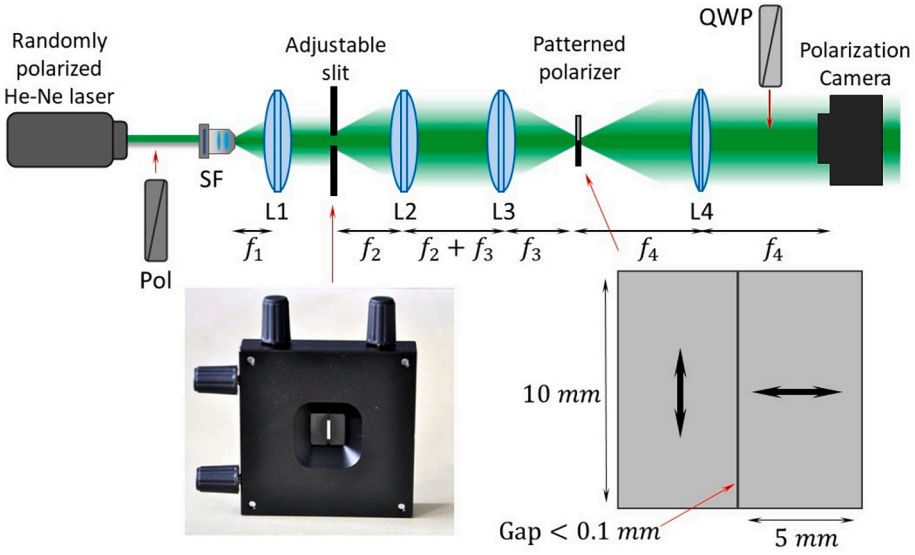

Fig. 5. Experimental setup. An adjustable slit is imaged onto a double rectangular polarizer. Pol (linear polarizer), SF (spatial filter), L (lens), QWP (quarter-wave plate).

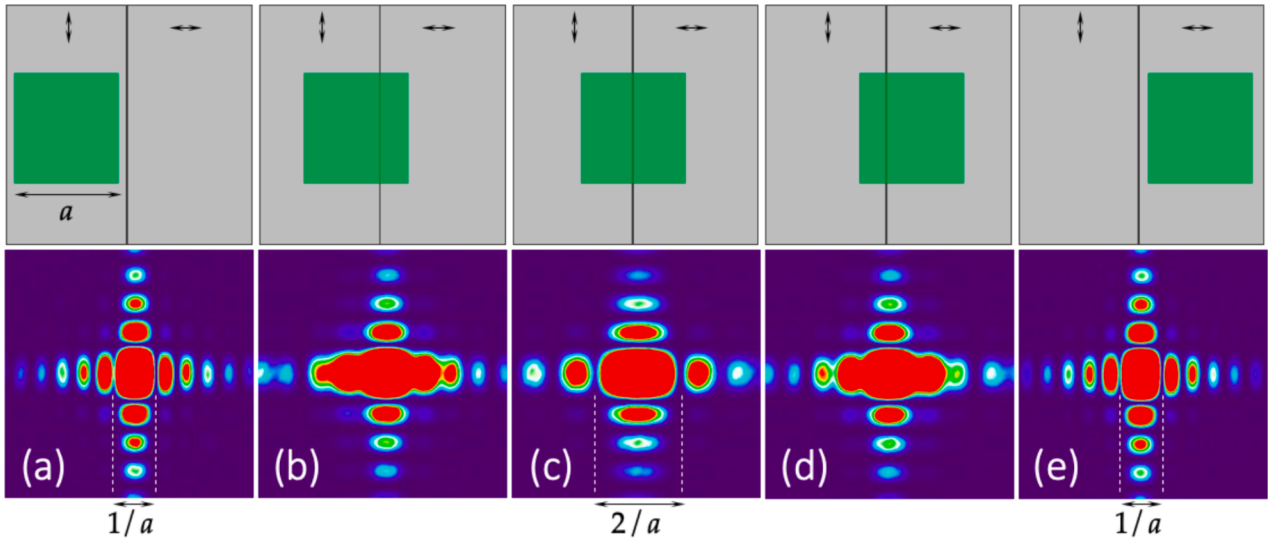

Fig. 6. Top: Scheme of the alignment of the slit image (green rectangle) onto the double polarizer. Bottom: Experimental diffraction pattern captured without analyzer. When the image of the slit lies in the middle of the double polarizer, the sinc pattern doubles its size. (For interpretation of the references to colour in this figure legend, the reader is referred to the web version of this article.). (For interpretation of the references to colour in this figure legend, the reader is referred to the web version of this article.). (For interpretation of the references to colour in this figure legend, the reader is referred to the web version of this article.)

Fig. 6 illustrates the alignment of the slit image onto the double polarizer. In this experiment, we insert the input polarizer (Pol) into the system. As a result, the input light beam impinging onto the adjustable slit is fully polarized with linear diagonal polarization (45°), although equivalent results are obtained if the input is unpolarized. The bottom row shows the intensity of the diffracted field measured at the camera as the image of the adjustable slit shifts laterally along the double polarizer. The schemes on the top row illustrate the corresponding location of the slit image (green rectangle) relative to the double polarizer element.

The results in Fig. 6(a), 6(c) and 6(e) clearly show the sinc square pattern characteristic of the diffraction from a rectangular aperture. Note that we intentionally saturated the camera in the central part, to clearly visualize the whole diffraction pattern. However, the scale of the sinc function along the horizontal direction is different when the light fully passes through one single polarizer (Fig. 6(a) and Fig. 6(e)), with respect to the case in Fig. 6(c), where the slit image lies just in the middle of the two polarizers. In Fig. 6(a) and 6(e), light emerging from all points of the rectangular aperture (whose horizontal width is a) all have the same polarization. In this situation, the expected diffracted field is that of the full aperture.

Hence, the width of the central lobe of the sinc function is proportional to $1/a$, as indicated in Fig. 5(a) and 5(e). On the contrary, as discussed in Section 2, when the left part of the aperture is vertically polarized and the right part is horizontally polarized, the scale of the sinc function doubles along the horizontal direction. As a result, the width of the central lobe is proportional to $2/a$ (Fig. 6(c)). At intermediate situations, as shown in Fig. 5(b) and 5(d), one polarization area is wider than the other and the diffracted field presents an intermediate pattern.

Next, the system was set with the slit image aligned with the double polarizer (as in Fig. 6(c)), and the polarization of the diffracted far field is analyzed. For that purpose, we captured the intensity pattern analyzed

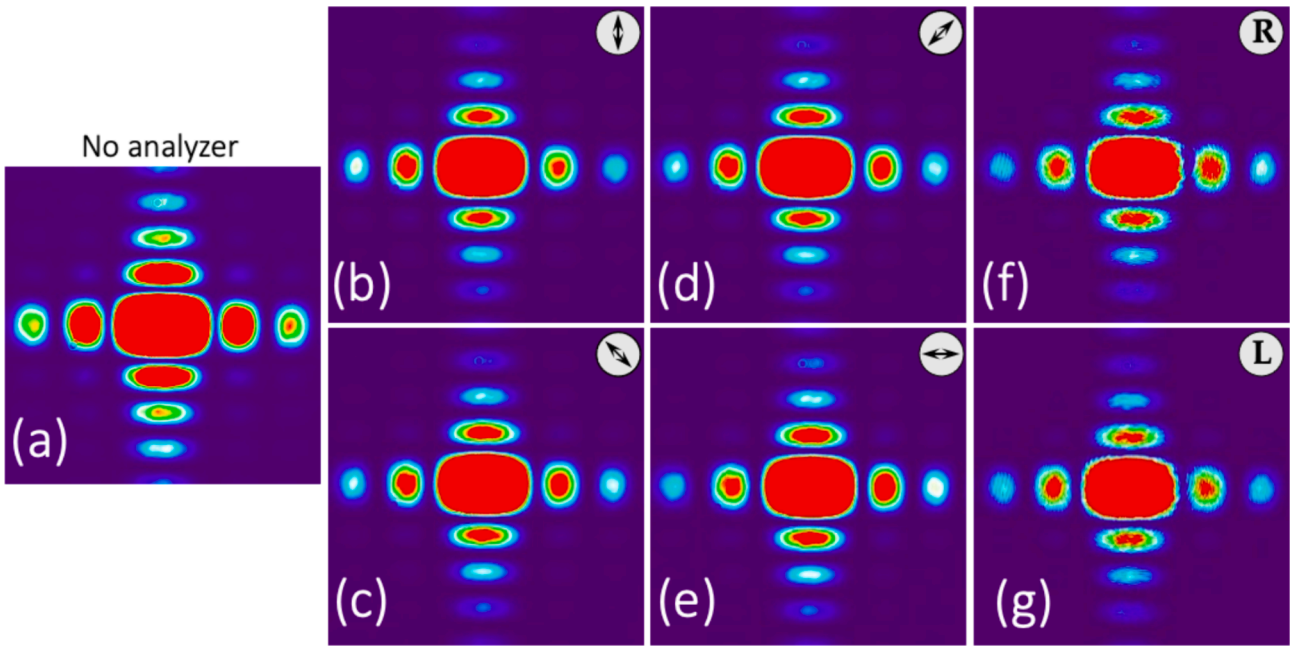

Fig. 7. Intensity of the diffracted field when the aperture is illuminated with unpolarized light. (a) No analyzer. (b-e) Linear polarizer analyzer with vertical, diagonal, antidiagonal, and horizontal orientations. (f-g) Circular polarizer analyzers.

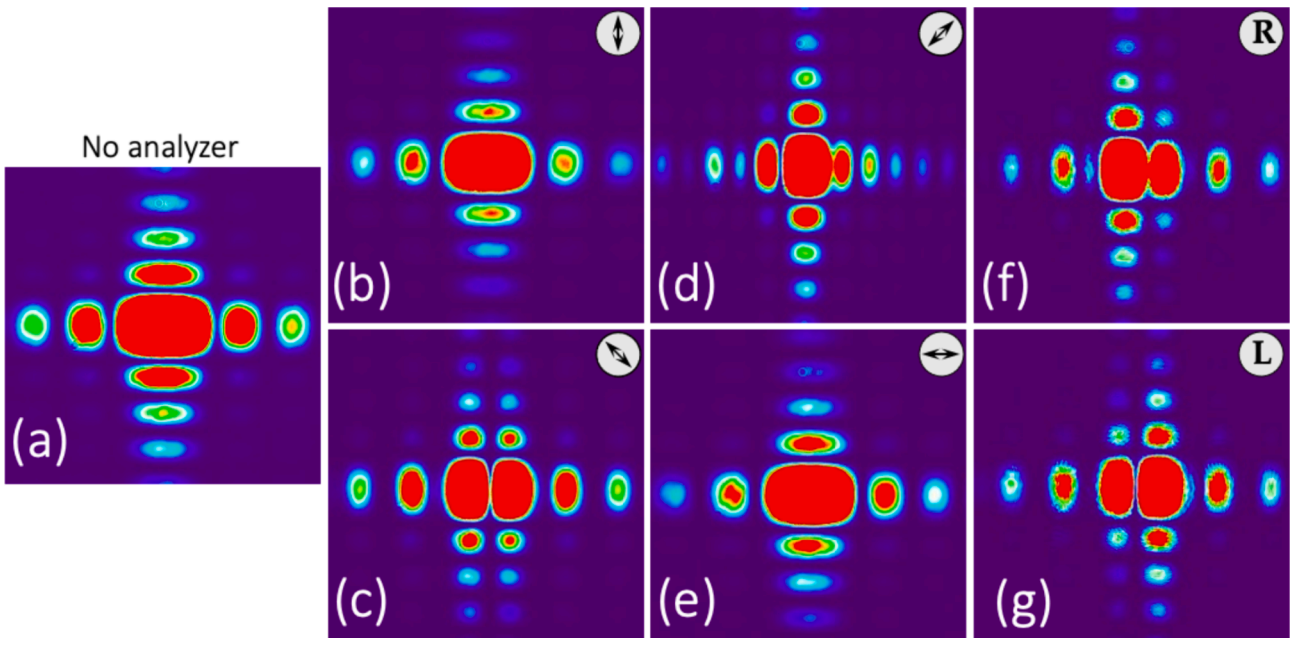

Fig. 8. Intensity of the diffracted field when the aperture is illuminated with linearly polarized light oriented at 45°. (a) No analyzer. (b-e) Linear polarizer analyzer with vertical, diagonal, antidiagonal, and horizontal orientations. (f-g) Circular polarizer analyzers.

by linear polarizers (oriented horizontal, vertical, diagonal and antidiagonal), and by right and left circular polarizers. The results are shown in Fig. 7 for unpolarized input light and in Fig. 8 for input light linearly polarized at 45°. The intensity captures without analyzer (Fig. 7(a) and 8 (a)) reveal the same sinc squared pattern in both cases. However, clear differences are visible in the polarization content.

In the first case (unpolarized input light), Fig. 7 shows the same intensity pattern for all analyzers, thus revealing that the diffracted field is unpolarized. Although the light is polarized by the polarizers in the aperture, the lack of coherence between points from each lateral polarizer produces this effect, as explained at the end of Section 4. On the contrary, the diffraction pattern behind the different polarization analyzers changes notably when the input beam is linearly polarized, as Fig. 8 shows. When the linear analyzer is oriented vertical or horizontal (Fig. 8(b) and 8(e)), the diffraction pattern retains the same shape as without analyzer (Fig. 8(a)). This can be understood as only the contribution from one rectangular polarizer is transmitted to the detector. Since the width of this single rectangular aperture is $a/2$, the corresponding sinc squared function central lobe width is proportional to $2/a$. When the linear analyzer is oriented diagonal at 45°, i.e., the same orientation as the input polarization, the resulting diffraction pattern is again the sinc squared function (Fig. 8(d)), but now the width of the central lobe is reduced to $1/a$. Since the input beam is fully polarized and has transverse spatial coherence, there is full correlation

between the light transmitted by the points on the left and on the right polarizer. Therefore, when projected onto a linear analyzer with 45° orientation, the whole rectangular behaves equivalently to a single aperture of width a illuminated with a coherent beam. When the linear analyzer is oriented antidiagonal at −45° (Fig. 8(c)), now the center becomes dark and the central lobe splits in two lateral lobes. Finally, for the circular analyzers (Fig. 8(f) and 8(g)), the splitting is asymmetric. All these results show an excellent agreement with the expected profiles shown in Fig. 1(c).

Producing a binary uncorrelated scalar spatial pattern

Now, let us consider the double polarizer rectangular aperture in Fig. 2(a), but this time, covered behind it with an additional linear polarizer oriented at 45°. As a result, the vectorial problem is transformed into a scalar one (the polarization is the same now over the whole aperture). If the aperture is now illuminated with the quasi-monochromatic unpolarized plane wave, the effective resulting aperture consists of two equally intense rectangles each with a width of $a/2$. Each rectangle contains fully coherent points, but the points in the left rectangle are fully incoherent with those in the right rectangle. The lack of correlation between the vertical and horizontal polarization components emerging from each side of the double rectangular aperture is now transformed into a lack of correlation between the scalar fields at the left and the right rectangles.

This example illustrates a simple way of generating a binary uncorrelated scalar spatial pattern: the binary pattern must be encoded in the orientation of a patterned polarizer with zones oriented either at 0° or 90°; then, by illuminating it with unpolarized light and placing a linear polarizer behind it oriented at 45°, the two regions become spatially uncorrelated.

We experimentally select this configuration for the double polarizer rectangular aperture, which provides an intensity distribution as the one shown in Fig. 7(d). The BCP matrix $\widehat{J}_2(u_a,u_b)$ in Eq. (29) that describes the diffracted field must be now modified by the presence of the additional polarizer with 45° orientation, leading to a new BCP matrix:

$$\widehat{J}'_2(u_a,u_b)=\frac{1}{2}\begin{pmatrix}1&1\\1&1\end{pmatrix}\widehat{J}_2(u_a,u_b)\frac{1}{2}\begin{pmatrix}1&1\\1&1\end{pmatrix}=G(u_a,u_b)\frac{1}{2}\begin{pmatrix}1&1\\1&1\end{pmatrix}. \tag{32}$$

As expected, Eq. (32) shows that the polarization is a uniform linear state oriented at 45°, with the maximum degree of polarization. The function $G(u_a,u_b)$ is the mutual intensity, now the same in all matrix elements, which is given by:

$$G(u_a,u_b)=\frac{a^2}{8}\mathrm{sinc}\left(\frac{au_a}{2}\right)\mathrm{sinc}\left(\frac{au_b}{2}\right)\cos\left[\frac{\pi a}{2}(u_a-u_b)\right]. \tag{33}$$

The intensity is $I(u)=(a^2/8)\mathrm{sinc}^2(au/2)$, i.e., equal to Eqs. (11) and (31) except for a 1/2 factor due to the absorption at the added polarizer. The complex degree of coherence is:

$$g(u_a,u_b)=\frac{G(u_a,u_b)}{\sqrt{I(u_a)I(u_b)}}=\\ =\mathrm{sgn}\left[\mathrm{sinc}\left(\frac{au_a}{2}\right)\mathrm{sinc}\left(\frac{au_b}{2}\right)\right]\cos\left[\frac{\pi a}{2}(u_a-u_b)\right], \tag{34}$$

where sgn[•] indicates the signum function. The correlation is maximum when $u_a-u_b=2m/a$, while it is null when $u_a-u_b=2(m+1/2)/a$, where m represents integer values.

To verify these properties, we modified the experimental setup in Fig. 5 by placing a liquid–crystal on silicon (LCOS) spatial light modulator (SLM) in the Fourier transform plane, as indicated in Fig. 9(a). The SLM is from Santec, model SLM-100–01–0001–12, with 1440 × 1050 pixels and a pixel size of 10.0 μm × 10.4 μm. It is used to display a uniform image except within two narrow rectangles having width Δ and separated a distance d, as shown in Fig. 8(b). These two rectangles display blazed diffraction gratings, thus acting as two slits that diffract light in the vertical direction. The reflected beam is then directed to another converging lens that performs another Fourier transform which is focused onto the camera. Fig. 8(c) shows an experimental example of what it is observed in the camera. The bottom part shows a highly saturated distorted image of the double polarizer rectangle aperture, while the upper part shows the characteristic interference pattern generated by two narrow slits. The predictions in Eq. (34) can be verified by measuring the visibility of these interference fringes through modifying the location of the slits displayed on the SLM.

In the experiments, we used two slits located symmetrically with respect to the center of the diffracted field, as shown in Fig. 9(b), i.e., $u_a=u$ and $u_b=-u$. This arrangement allowed us to select two lateral positions of the diffracted field with equal intensity, with a slit separation of $d=2u$. For these positions the modulus of the complex degree of coherence follows:

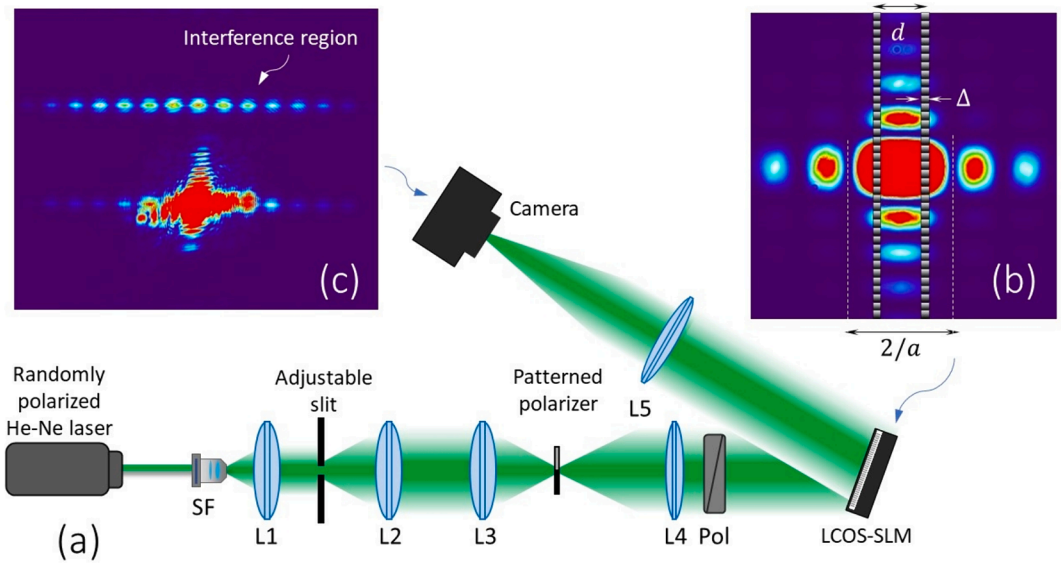

Fig. 9. (a) Modified experimental setup where a SLM is included in the Fourier transform plane. (b) A double slit blazed grating is displayed on the SLM. (c) Experimental capture at the camera detector showing the interference pattern.

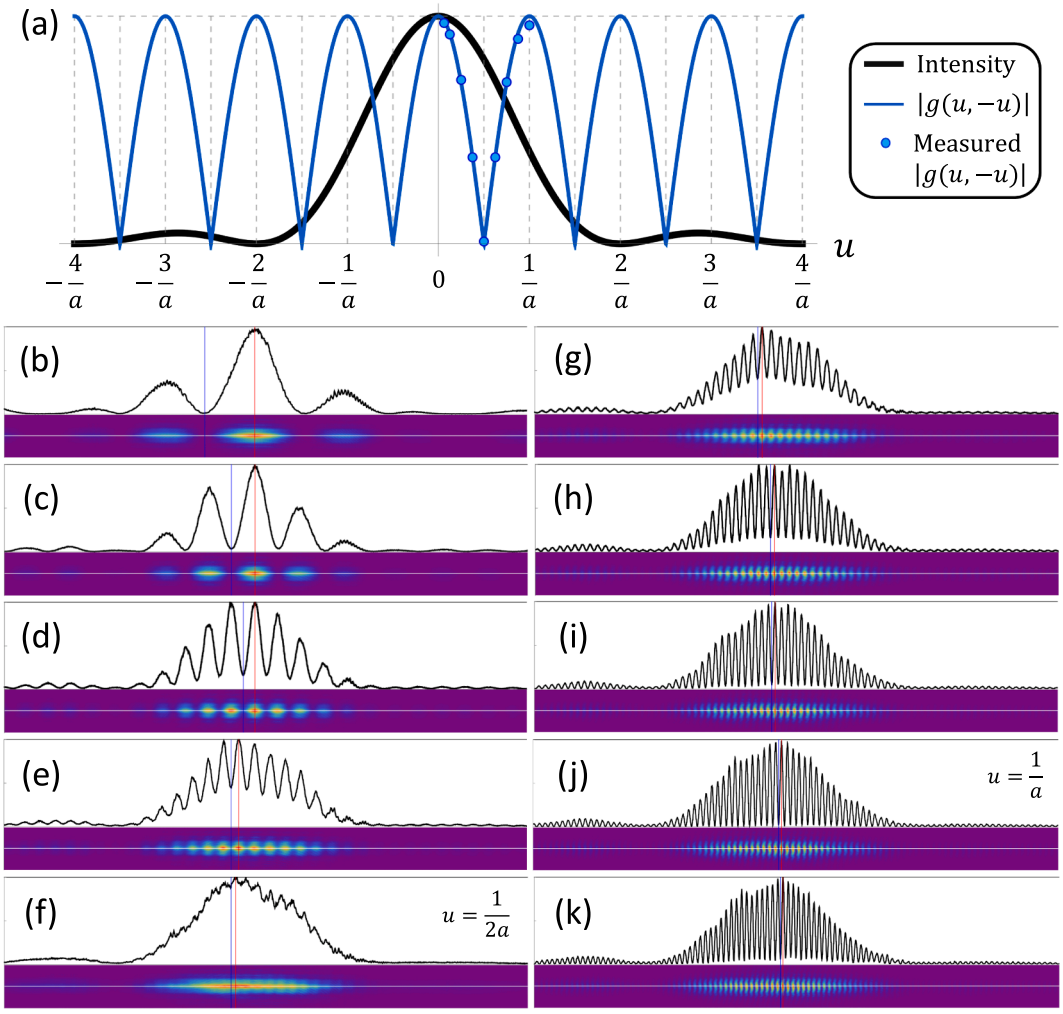

Fig. 10. (a) Theoretical curves for the intensity and for the absolute value of complex degree of coherence $|g(u,-u)|$ of the diffracted field generated by the double incoherent rectangular aperture. The figure also includes the measured $|g(u,-u)|$. (b)-(k) Intensity measurements in the interference region as the distance between slits increases. Red and blue vertical lines indicate the location of $I_{\max}$ and $I_{\min}$ to calculate the visibility. (For interpretation of the references to colour in this figure legend, the reader is referred to the web version of this article).

$$|g(u_a = u, u_b = -u)| = |\cos(\pi a u)|. \tag{35}$$

Fig. 10(a) illustrates the profile of the function $\mathrm{sinc}^2(au/2)$, which represents the expected intensity generated by the double incoherent rectangular aperture, normalized to its maximum value, together with the modulus of the expected complex degree of coherence at $|g(u,-u)|$. Within the central lobe of the sinc squared function, $|g(u,-u)| = 1$ at $u = 0$, which is trivial since the same point is considered. Additionally, $|g(u,-u)| = 1$ also when the two slits are placed at $u = \pm 1/a$. In between, $|g(u,-u)|$ is reduced, becoming null when $u = 1/(2a)$ and $u = 3/(2a)$.

The corresponding verification is illustrated in the experimental captures shown in Fig. 10. The slits have a width of $\Delta = 8$ pixels, so there is enough light being diffracted to the interference region. The blazed gratings inside have a small period of only 8 pixels, so the interference pattern is vertically shifted enough distance to be separated from the central image. The results in Fig. 10 show the cropped image area where the interference is observed, together with the corresponding intensity profile, normalized to the maximum value in each case.

Note that, because of the width Δ of the slits, the interference region has the shape of a sinc squared function. The captures in Fig. 10(b-k) present the interference patterns as we progressively increase the distance d between the two slits. The fringes are wide when the two slits are very close (Fig. 10(b)), and they become narrower as d increases. The other feature clearly observed is the change in the visibility of the fringes as d changes, as expected from Eq. (35). It is easy to identify when the slits are located at $u = \pm 2/a$ because there is no light in the interference region, since $I(u_a)$ is zero at these points. Then, the slits can be placed at $u = \pm 1/(2a)$ (Fig. 10(f)), where it is observed how the visibility is almost zero. Conversely, for $u = 1/a$ (Fig. 10(j)), the visibility of the fringes is almost one, in accordance with the result expected from Eq. (35).

The value of $|g|$ is determined experimentally from the visibility of the interference patterns in Fig. 9(b-m) and it is plotted in Fig. 9(a) for comparison with Eq. (35). Measurements are presented up to $u = 1/a$. Points beyond this range were not considered due to the low intensity and rapid variation of the fringes. To account for the sinc squared envelope resulting from the slits limited size, we also measured the intensity within the interference region when only one slit was displayed on the SLM. Since the slit width and the total intensity passing through each slit are the same, the diffraction pattern caused by each slit separately appears nearly identical. Consequently, $|g| = (I'_{\max} - I'_{\min})/(I'_{\max} + I'_{\min})$ where $I'_{\max,\min}$ are the intensity values at two adjacent maximum and minimum in the interferograms in Fig. 10, each one normalized by the intensity measured at the same points when a single slit is displayed. The red and blue vertical lines indicated on Fig. 9 (b)-(k) denote the location of $I_{\max}$ and $I_{\min}$ used to calculate the visibility.

Conclusions

In summary, we have considered an analytical problem proposed by Gori and coworkers [21], consisting in a rectangular aperture where the left half is a vertical linear polarizer while the right half is a horizontal linear polarizer, and we used it to illustrate the calculation of the diffracted field in the Fourier transform domain.

First, we analyzed it within the Fourier transform Jones (FTJ) matrix formalism [18]. The interesting feature of the FTJ matrix $\widehat{M}(\mathbf{u})$ is that it characterizes the diffractive element in the Fourier domain, thus including the polarization transformation at the PDOE plane and the polarization transformation due to the propagation. When the PDOE is illuminated with a uniformly polarized plane wave $\widehat{M}(\mathbf{u})$ directly provides the diffracted field simply by multiplying it by the input Jones vector. If the input wave is not a plane wave, the diffracted field is given by the convolutional relation in Eq. (5). This expression can be simplified (Eq. (6)) when the input beam is scalar. We provided the analytical expression for the FTJ matrix describing the double polarizer rectangular aperture illuminated with a plane wave and used it to derive relations of the intensity and the local state of polarization on the diffracted field. However, this approach holds only for fully polarized light that is spatially coherent.

On the other hand, the BCP matrix [11] is a powerful formalism to analyze PDOE, which can be applied to input beams with arbitrary polarization and coherence properties. We derived a general relation (Eq. (21)) of the BCP matrix in the FT domain, resulting in double convolution functions involving the FTJ matrix $\widehat{M}(\mathbf{u})$. The result becomes particularly simple when the PDOE is illuminated with an input scalar partially polarized field with transverse spatial coherence. When the incident state is a partially polarized plane wave of uniform polarization, the relation further simplifies, since it results in the usual BCP transformation rule using $\widehat{M}(\mathbf{u})$ (Eq. (23)). But note that other illumination situations can be considered using the general relation in Eq. (21).

There are methods for the experimental fully determination of the BCP matrix [32]. Here, instead, we use intensity measurements of the diffraction pattern generated by a simple double polarizer rectangular aperture that evidence the different correlations between the electric field components. We compare the diffraction when the double polarizer rectangular aperture is illuminated with spatially coherent input beam but different polarizations: 1) fully polarized linear polarization oriented at 45°, and 2) completely unpolarized input beam. For each case, we applied the combined BCP-FTJ approach to calculate the intensity and polarization spatial distribution in the Fourier plane. The polarization distribution right after the aperture is the same in both cases, and the intensity of the diffracted field is also the same. However, the polarization distribution at the diffraction plane is very different: while in the first case the polarization state changes with the spatial frequency, in the second case the diffraction pattern is completely unpolarized. This behavior is explained by the fact that the two orthogonal linearly polarized fields diffracted by each polarizer in the aperture are totally correlated in the first case, whereas they are totally uncorrelated in the latter. We also noted the analogy of this double polarizer rectangular aperture with the case of a circular aperture with two radial regions with orthogonal polarizers which, after a convenient coordinate transformation, it is shown to produce an equivalent behavior along the propagation axis.

An experiment to verify the results was designed, where we used a patterned polarizer. A Fourier optics setup was built, with a randomly polarized He-Ne laser as light source and a polarization camera that captures polarimetric images of the diffracted field. The diffraction pattern in the Fourier domain has been analyze experimentally, analyzing not only the intensity but also the state of polarization by means of a polarization camera. The experiments confirm all the theoretical predictions.

A final experiment is also included where we measure the coherence between points of the diffracted field in the case where a polarizer oriented at 45° is included after the aperture. This experiment illustrates how by employing a suitable patterned binary polarizer illuminated with randomly polarized light, becomes feasible to attain a desired binary spatial coherence pattern while preserving the field's amplitude and phase functions of a scalar field unaltered. Moreover, the laser's rapid depolarization dynamics offers a faster alternative to digital micromirror devices [24] for achieving spatial coherence patterns. Exploring spatial coherence patterns beyond binary would involve employing spatially variant polarizers with more than two orientations. This results in intensity loss in certain regions upon traversing the second polarizer, depending on the desired coherence function. Compensating for this loss would require a more sophisticated experiment.

The emergence of new PDOEs based on metamaterials and spatially patterned liquid-crystals is pushing the applications of structured light. We envisage that this framework could be useful in this field since it provides a mathematical tool for analyzing the performance of such metasurface and geometric phase diffractive elements.

Funding

This work was financed by Ministerio de Ciencia e Innovación, Spain (refs.: PID2021-126509OB-C22, and −C21 and PDC2022-133332-C22) and Generalitat Valenciana (ref. CIAICO/2021/276). D. M. acknowledges Ministerio de Universidades, Spain, Universidad Miguel Hernández and the European Union (Next generation EU fund) for a Margarita Salas grant from the program Ayudas para la Recualificación del Sistema Universitario Español.

CRediT authorship contribution statement

Ignacio Moreno: Writing – review & editing, Project administration, Investigation, Conceptualization. **David Marco:** Writing – review & editing, Methodology, Investigation, Formal analysis. **María del Mar Sánchez-López:** Writing – original draft, Validation, Formal analysis. **Juan Campos:** Writing – review & editing, Supervision, Formal analysis, Conceptualization. **Angel Lizana:** Writing – review & editing, Validation, Formal analysis.

Declaration of competing interest

The authors declare that they have no known competing financial interests or personal relationships that could have appeared to influence the work reported in this paper.

Data availability

Data will be made available on request.

References

[1] Piquero G, Martínez-Herrero R, de Sande JCG, Santarsiero M. Synthesis and characterization of non-uniformly polarized light beams: tutorial. J Opt Soc Am A 2020;37(4):591–605. https://doi.org/10.1364/JOSAA.379439.
[2] Rubin NA, Shi Z, Capasso F. Polarization in diffractive optics and metasurfaces. Adv Opt Photon 2021;13(4):836–970. https://doi.org/10.1364/AOP.439986.
[3] Beresna M, Kazansky PG. Polarization diffraction grating produced by femtosecond laser nanostructuring in glass. Opt Lett 2010;35(10):1662–4. https://doi.org/10.1364/OL.35.001662.
[4] Khorasaninejad M, Chen WT, Zhu AY, Oh J, Devlin RC, Roques-Carmes C, et al. Visible wavelength planar metalenses based on titanium dioxide. IEEE J Select Top Quant Electron 2017;23(3):4700216. https://doi.org/10.1109/JSTQE.2016.2616447.
[5] Sun Y, Liu Y, Wu T, Li J, Fan H, Wang X. Polarization-dependent metalens with flexible and steerable bifocal spots. Results Phys 2023;46:106286. https://doi.org/10.1016/j.rinp.2023.106286.
[6] Rubano A, Cardano F, Piccirillo B, Marrucci L. Q-plate technology: a progress review. J Opt Soc Am B 2019;36(5):D70–87. https://doi.org/10.1364/JOSAB.36.000D70.

[7] Rubin NA, Zaidi A, Dorrah AH, Shi Z, Capasso F. Jones matrix holography with metasurfaces. Sci Adv 2021;7:eabg7488. https://doi.org/10.1126/sciadv.abg7488.
[8] Feng C, He T, Shi Y, Song Q, Zhu J, Zhang J, et al. Diatomic metasurface for efficient six-channel modulation of Jones matrix. Laser & Photon Rev 2023;17:2200955. https://doi.org/10.1002/lpor.202200955.
[9] Zhao R, Wei Q, Li Y, Li X, Geng G, Li X, et al. Stereo Jones matrix holography with longitudinal polarization transformation. Laser & Photon Rev 2023;17:2200982. https://doi.org/10.1002/lpor.202200982.
[10] He C, Shen Y, Forbes A. Towards higher-dimensional structured light. Light Sci & Appl 2022;11:205. https://doi.org/10.1038/s41377-022-00897-3.
[11] Gori F, Santarsiero M, Vicalvi S, Borghi R, Guattari G. Beam coherence-polarization matrix. Pure Appl Opt 1998;7:941–51. https://doi.org/10.1088/0963-9659/7/5/004.
[12] Wolf E. Introduction to the Theory of Coherence and Polarization of Light. Cambridge University Press; 2007.
[13] Piquero G, Borghi R, Santarsiero M. Gaussian Schell-model beams propagating through polarization gratings. J Opt Soc Am A 2001;18(6):1399. https://doi.org/10.1364/JOSAA.18.001399.
[14] Santarsiero M, de Sande JCG, Piquero G, Gori F. Coherence-polarization properties of fields radiated from transversely periodic electromagnetic sources. J Opt 2013;15:055701. https://doi.org/10.1088/2040-8978/15/5/055701.
[15] Visser TD, Agrawal GP, Milonni PW. Fourier processing with partially coherent fields. Opt Lett 2017;42(22):4600–2. https://doi.org/10.1364/OL.42.004600.
[16] Zhao X, Visser TD, Agrawal GP. Controlling the degree of polarization of partially coherent electromagnetic beams with lenses. Opt Lett 2018;43(10):2344–7. https://doi.org/10.1364/OL.43.002344.
[17] Wang Y, Yan S, Li X, Liu X, Cai Y, Agrawal GP, et al. Fraunhofer diffraction and the state of polarization of partially coherent electromagnetic beams. Opt Lett 2019;44(13):3330–3. https://doi.org/10.1364/OL.44.003330.
[18] Moreno I, Yzuel MJ, Campos J, Vargas A. Jones matrix treatment for polarization Fourier optics. J Mod Opt 2004;51(14):2031–8. https://doi.org/10.1080/09500340408232511.
[19] Moreno I, Iemmi C, Campos J, Yzuel MJ. Jones matrix treatment for optical processors with structured polarization. Opt Express 2011;19(5):4583–94. https://doi.org/10.1364/OE.19.004583.
[20] Rubin N, D'Aversa G, Chevalier P, Shi Z, Chen WT, Capasso F. Matrix Fourier optics enables a compact full-Stokes polarization camera. Science 2019;365:eaax1839. https://doi.org/10.1126/science.aax1839.
[21] Dorrah AH, Rubin NA, Zaidi A, Tamagnone M, Capasso F. Metasurface optics for on-demand polarization transformations along the optical path. Nature Photon 2021;15:287–96. https://doi.org/10.1038/s41566-020-00750-2.
[22] Gori F, Santarsiero M, Borghi R, Guattari G. The irradiance of partially polarized beams in a scalar treatment. Opt Commun 1999;163:159–63. https://doi.org/10.1016/S0030-4018(99)00130-3.
[23] Shevchenko A, Roussey M, Friberg AT, Setälä T. Polarization time of unpolarized light. Optica 2017;4(1):64. https://doi.org/10.1364/OPTICA.4.000064.
[24] Rodenburg B, Mirhosseini M, Magaña-Loaiza OS, Boyd RW. Experimental generation of an optical field with arbitrary spatial coherence properties. J Opt Soc Am B 2014;31(6):A51–5. https://doi.org/10.1364/JOSAB.31.000A51.
[25] Wang F, Liu X, Yuan Y, Cai Y. Experimental generation of partially coherent beams with different complex degrees of coherence. Opt Lett 2013;38(11):1814–6. https://doi.org/10.1364/OL.38.001814.
[26] Goodman JW. Introduction to Fourier Optics. 3rd Edt,. Roberts & Company Publishers; 2005.
[27] Martinez-Corral M, Andrés P, Ojeda-Castañeda J, Saavedra G. Tunable axial superresolution by annular binary filters. Application to confocal microscopy. Opt Commun 1995;119:491–8. https://doi.org/10.1016/0030-4018(95)00380-Q.
[28] Davis JA, Pascoguin ML, Tuvey CS, Cottrell DM. Fourier transform pupil functions for modifying the depth of focus of optical imaging systems. Appl Opt 2009;48(26):4893–8. https://doi.org/10.1364/AO.48.004893.
[29] Moreno I, Iemmi C, Campos J, Yzuel MJ. Binary polarization pupil filter: Theoretical analysis and experimental realization with a liquid crystal display. Opt Commun 2006;264:63–9. https://doi.org/10.1016/j.optcom.2006.02.016.
[30] https://www.codixx.de/en/home.
[31] Nabadda E, Sánchez-López MM, Vargas A, Lizana A, Campos J, Moreno I. Mueller matrix imaging polarimeter with polarization camera self-calibration applied to structured light components. J Eur Opt Soc - RP 2024;20:5. https://doi.org/10.1051/jeos/2024003.
[32] Kanseri B, Rath S, Kandpal HC. Determination of the beam coherence-polarization matrix of a random electromagnetic beam. IEEE J Quant Electron 2009;45(9):1163–7. https://doi.org/10.1109/JQE.2009.2020178.